Additive Manufacturing 79 (2024) 103926

Contents lists available at ScienceDirect

Additive Manufacturing

journal homepage: www.elsevier.com/locate/addma

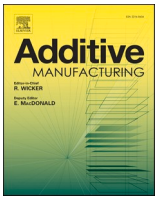

Study of Proximity Effect in Projection based Micro Vat Photopolymerization Process

Aditya Chivate, Zipeng Guo, Chi Zhou *

Department of Industrial and Systems Engineering, University at Buffalo, The State University of New York, Buffalo, NY 14260, USA

ARTICLE INFO

Keywords:
Proximity effects
Oxygen inhibition
Cross-talk
Vat photopolymerization

ABSTRACT

Micro Projection-based Stereolithography (μPSL), also known as micro vat photopolymerization, is a promising technology that could revolutionize microfabrication by providing benefits similar to traditional lithography while reducing production time and cost. However, it faces a significant challenge in the form of the "proximity effect." This effect occurs when adjacent features are too close together, causing undesirable artifacts and limiting the achievable fabrication resolution. The proximity effect is caused by interactions between adjacent pixels of light and affects both the spatial and temporal domains of the fabrication process. Although researchers have been aware of this issue for some time, there has been little progress in understanding and addressing the proximity effect in micro vat photopolymerization. Existing models developed for laser-based systems can explain the effect to some extent, but they do not fully account for the impact of large area projection or explain how local threshold changes affect part size. This research aims to fill this knowledge gap by using in-situ observation systems to experimentally study the spatial and temporal proximity effects in single-shot vat photopolymerization microfabrication. We also investigate the role of oxygen in the proximity effect and lay the groundwork for better understanding how the effect impacts periodic structures with micronic inter-feature distances. In conclusion, while micro vat photopolymerization offers significant advantages over traditional lithography, the proximity effect remains a significant obstacle. This research represents an important step forward in addressing this challenge and improving the accuracy and resolution of vat photopolymerization in microfabrication.

1. Introduction

Additive manufacturing, also known as 3D printing, has revolutionized the way we fabricate things and has found applications in various fields such as biomedical devices, automotive components, photonics, micromechanics, microbiology, targeted drug delivery, and optics [1–6]. Cutting-edge technological advancements in additive manufacturing have unlocked the ability to produce intricate micron-scaled features, allowing for unprecedented precision in the fabrication of objects. Furthermore, this breakthrough has extended to the realm of biologically inspired textured surfaces, enabling the creation of patterned structures that mimic the complexity and functionality found in nature. Two-Photon Polymerization (2PP) has long been used for fabricating sub-micron features, but its slow print speed of 10 μm/s has led researchers to search for alternatives [7]. Despite the efforts made in mass parallelization, the high costs associated with the tools make their entry into the industrial setting challenging [8,9]. Digital Light Projection (DLP) based vat photopolymerization uses a series of digital masks to fabricate high resolution 3D structures. As it is based on the projection of a complete image at each instance, the build area depends on the projection size and can thus be easily manipulated by changing the projection optics for desired magnification. Vat photopolymerization has seen a considerable push in its benchmarks in recent years and has the potential to overtake 2PP due to its high throughput and economic setup costs [10]. Densely packed high-resolution features are desirable in microfabrication [1]. The features resolution depends on the size of the illuminated pixel and can be scaled by using appropriate optics. However, generating tiny freestanding features and reducing feature separation remains challenging. Oxygen diffusion limits the feature size whereas high density packing leads to abnormal stretching and sporadic interconnects between the features. The loss in feature resolution due to propinquity is termed "proximity-effect" [11,12]. Proximity effect in vat photopolymerization based printing is a complex phenomenon that cannot be attributed to a single mechanism. A number

* Corresponding author.
E-mail address: chizhou@buffalo.edu (C. Zhou).

https://doi.org/10.1016/j.addma.2023.103926
Received 17 July 2023; Received in revised form 29 October 2023; Accepted 12 December 2023
Available online 14 December 2023

of potential reasons contributing to the proximity effect could include the chemical properties of the polymer, light scattering and spreading, thermal or molecular diffusion, dose addition due to subsequent projections, and oxygen inhibition [13]. However, there is neither a precise knowledge about the underlying mechanisms of proximity effect, nor is the effect well characterized in strength or spatial-temporal domain typical to vat photopolymerization based printing.

Theoretically, local polymerization in vat photopolymerization should occur only in the irradiation region. However, in practice, the phenomenon of light bleeding in neighboring pixels during local polymerization in Digital Light Processing (DLP) can lead to the formation of a partially cured resin envelope around the desired feature [14]. Two primary reasons may cause this over-exposure; either the time delay between two subsequent exposures is too small for the oxygen to replenish, or the gap between the adjacent features is smaller than the light bleeding threshold. If the cross-talking between the features occurs due to the closeness of the features, it is termed as "spatial proximity effect"; if it occurs because of the time delay between subsequent projections, it is termed as "temporal proximity effect." While these effects have been studied in projection stereolithography, most research has been conducted at macro scale. For instance, Zhou and others have laid the groundwork for understanding pixel blending and have introduced optimization methods for grayscale pixel illumination [15,16]. Kang and colleagues have developed mathematical models that provide further insights into pixel-based solidification during photopolymerization, supported by thorough experimental validation [17]. These models offer a reliable means of predicting voxel growth while considering light bleeding. Emami's work on comprehending the energy profile of individual pixels builds upon Sun's previous research on modeling the first-order Gaussian nature of light from each pixel and the superposition effect of several illuminated micromirrors [18–21]. This elucidates how energy is distributed at the individual pixel level, forming a basis for understanding energy mapping in projection stereolithography. These effects are present across scales but are detrimental, especially in micron-scaled patterned structures, where precise feature definition and resolution are crucial. Efforts to address and mitigate this proximity effect in projection based photopolymerization are crucial for achieving high-fidelity microfabrication. Ongoing efforts include exposure time optimizations and grayscale mask generation strategies. More recently, Montgomery et al. has explored the use of grayscaling to enhance feature resolution. The reaction-diffusion simulation used in this work establishes a basis for parameter optimization to improve feature size, potentially leading to robust 3D curing models [22]. Quantifying these effects through rigorous observations can provide a deeper understanding of the underlying mechanisms.

Another aspect of studying the proximity effect involves understanding the chemical kinetics of the photopolymerization process. Over the years, significant progress has been made in comprehending the photopolymerization kinetics of acrylate-based resins. Researchers have discussed not only the well-established long-chain polymerization process with initiation and termination reactions but also the impact of oxygen diffusion [23]. The numerical simulations outlined by Taki and others have been foundational in understanding the chemical kinetics within the proximity effect at the microscale [24], as explored in our present study. While we considered the oxygen inhibition model from their work in designing our experiments, our research primarily focuses on acknowledging and qualitatively studying the effect, rather than quantifying it.

The research aims at using novel observation tools to observe the proximity effect and how it affects the voxel growth process, to quantitatively characterize the strength of the proximity effect on spatial and temporal scales specific to vat photopolymerization at micron scale, develop simulations to predict voxel growth based on the characterized proximity effect, and to design strategies for fabricating high resolution parts with high feature density using optimized multi-exposure strategy. The research uses a DMD light modulator to precisely control the mask shapes and inter-feature spacing. The impact of spatial distribution on the photopolymerization process is studied, and a general decay function is derived based on the collected data. Multi-mask projection strategies to circumvent the spatial proximity effect are presented, and the temporal effect arising due to the time delay between the exposures is studied. The research hypothesizes that oxygen plays a vital role in determining the extent of the proximity effect and presents experimental evidence of the effect of oxygen. In the case of our work, which deals with micron-scaled features, thermal changes in the vat were found to be insignificant in preliminary experiments and thus fall beyond the scope of our investigation. Voxel growth simulations based on Beer-Lambert's law and photopolymerization kinetics incorporating the proximity effect are developed. The paper also proposes multi-mask projection strategy for high resolution microlens fabrication.

The growing interests in miniaturizing of opto-electronics have led to a significant focus on developing micro-optical devices. These devices have found widespread applications in sensing, imaging, surface modifications, and electronics. Microlenses, which are tiny lenses with diameter typically under a millimeter, play a crucial role in these devices. The proximity effect, as explored in this paper, holds significant relevance in applications related to high-density microlens fabrication. This paper discusses how the studied proximity effect can be used for optimizing the fabrication strategies for high uniformity and resolution.

2. Theoretical modeling

Vat polymerization is the selective layer-by-layer polymerization of photosensitive resin utilizing ultraviolet (UV) light in the form of digital masks. This method outperforms the conventional galvo-mirror scanning method in speed and effectiveness. In order to project digital patterns onto the build plate more quickly, Digital Light Processing (DLP), which uses a spatial light modulator like an LCD screen or a digital micromirror device (DMD), uses parallel processing. The intensity of the irradiation, the wavelength, the chemical characteristics of the resin, and the input energy all affect the photopolymerization process. The photopolymerization process is influenced by a number of variables, including light intensity, wavelength, chemical characteristics of the resin, and input energy. Studying how light and resin interact, especially within the sphere of influence around the feature, is crucial for enhancing print resolution.

2.1. Light irradiance and light-resin interactions

Light irradiance controls the lateral resolution of vat photopolymerization process. Diffraction inefficiencies and dark-field diffusion caused by the projection device leads to a Gaussian distribution of the light projected off each pixel and causes the light to bleed into neighboring regions. Thus, the light energy received at each location is a result of the contribution of multiple surrounding pixels [25,26]. This region of impact surrounding the illuminated pixel is referred to as 'sphere of influence' in this research work. As the light distribution is Gaussian, the size of the sphere of influence dependent on the wavelength and intensity. Light intensity at each location (x, y) is governed by Eq. (1):

$$I(x,y,0) = \sum_{(x_i,\ y_j)\in\mathscr{S}} I_{i,j}\exp\left\{-\left[\left(\frac{x-x_i}{\sigma_x}\right)^2+\left(\frac{y-y_j}{\sigma_y}\right)^2\right]\right\} \tag{1}$$

where $(x_{\mathrm{i}},\ \ y_{\mathrm{j}}) \in \mathscr{S}$ is the location of the pixels, $I_{\mathrm{i,j}}$ is the light intensity at the pixel center, and σ_x and σ_y are the parameters that determine the spatial spread of the Gaussian profile. σ_x and σ_y are wavelength dependent and are positively corelated with the wavelength.

As the light intensity follows a 3D Gaussian distribution in free space, the vertical dimension of the curve is controlled by the optical properties of the media and, in this case, the chemical properties of the photo-

polymer resin. The vertical spread of the gaussian curve is constrained by the curing depth which largely depends on the chemical composition of the photopolymer resin and is governed by Beer-Lambert's equation [27].

$$C_d = D_p \ln\left(\frac{E}{E_c}\right), D_p = \frac{1}{\alpha}, \alpha = \alpha_{initiator} + \alpha_{absorber} \tag{2}$$

where C_d is the curing depth, D_p is the penetration depth which relates to the light absorption coefficient α, E is the exposed energy and E_c is the critical exposure below which the photopolymerization is absent. The exposure energy is a function of the light intensity and time. Combining Eqs. (1) and (2), the light intensity at any spatial location can be represented as

$$I(x, y, z) = I(x, y, 0)\exp\left\{-\frac{z}{D_p}\right\} \tag{3}$$

The total exposure energy is a function of intensity and time and is represented in 4D space by the following equation

$$E(x, y, z, t) = I(x, y, z)t \tag{4}$$

As the photopolymerization only takes place when the energy is greater than or equal to E_c, the shape and size of the cured profile can be computed by integrating Eqs. (1–4). For a single illuminated pixel, the shape of the cured profile is a paraboloid given by

$$x^2 + y^2 + z = D_p \ln\left(\frac{I_{\max}}{E_c}\right) \tag{5}$$

2.2. Photopolymerization simulation

Voxel growth simulations in photopolymerization were developed based on the aforementioned theories to study the effect of different parameters on the photopolymerization kinetics. Photopolymer simulations for a single voxel and the mechanics of pixel blending were discussed in the previous work [28]. The newly developed simulations utilize the same models while incorporating the effect of temporal and spatial proximity. For the purpose of the simulation, resin characteristics corresponding to the custom prepared PEGDA 250 based UV resin were considered. Experiments as discussed in Section 4 were performed to obtain the curing depth (C_d) and the critical energy (E_c) for the resin. As the energy distribution for each pixel is Gaussian, the energy spreads beyond the actual cured profile as shown in Fig. 1(a), where red color represents the exposed energy on the top surface of the resin and blue color represents the paraboloid profile of the cured part. The stray energy from adjacent features adds up and if the features are close together, which is represented by the overlapping red regions in Fig. 1 (a). Light bleeding into neighboring pixels has an additive effect and if the added energy crosses the threshold, it leads to the formation of interconnects. This is termed as spatial proximity effect and is more prevalent in the proximal region around the feature known as the sphere of influence. As seen in Fig. 1(a), a feature surrounded by other features tends to grow larger due to the contributions from its neighbors whereas the features on the corners retain the actual size.

Photopolymerization process involves quenching of oxygen free radicals before the initiation of short-chain polymerization. While Beer-Lambert's law has its merits, it falls short in explaining the interplay of oxygen or other physico-chemical elements during photopolymerization. Oxygen quenching takes place even beyond the feature size and the amount of quenched oxygen is a function on the irradiance. To address the effect of oxygen, we extended the Beer-Lambert's law by introducing an error term tailored to incorporate the effects of oxygen. We propose an advanced model to include the temporal proximity effect due to the influence of oxygen inhibition. Built upon the Beer-Lambert's law, we derived a more generalized form of the total energy exposure during time t where $\eta(t)$ represents the photopolymerization efficiency. Our preliminary studies have experimentally shown that photopolymerization process is highly nonlinear [28], and further experiments conducted in this work hint towards diffused oxygen being one of the influential factors. Dissolved oxygen scavenges the available free radicals inhibiting the polymerization process till its depletion. Thus, in

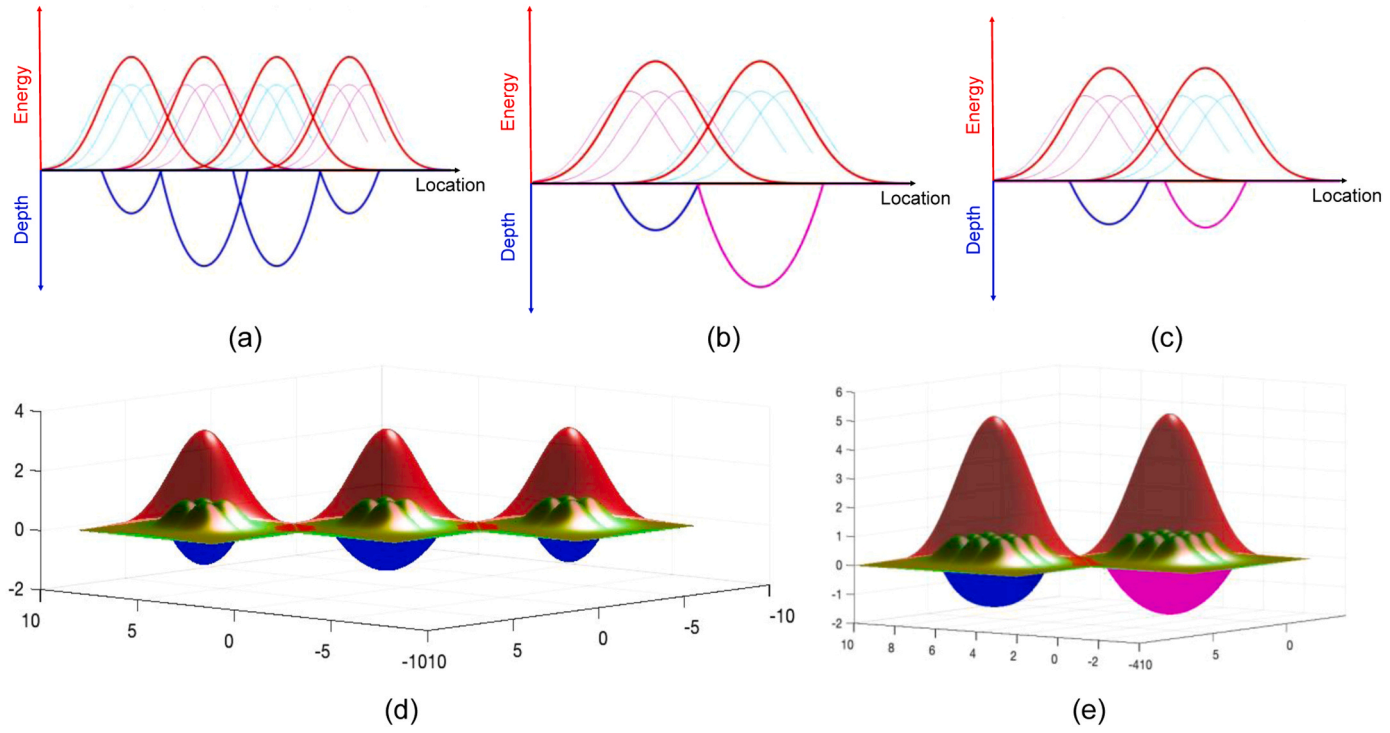

Fig. 1. Vat Photopolymerization simulation showing (a) spatial proximity effect, (b) temporal proximity effect when the time delay is short, and (c) temporal effect when the time delay is large. 3-D simulations showing the (d) Spatial proximity effect, and (e) Temporal proximity effect. Accumulated energy profile is shown by red curve, and the cured voxel is shown in blue and magenta.

the presence of oxygen the efficiency is a function of time and causes temporal complexity. Eq. (4) is modified as the integral of the intensity over time.

$$E(x,y,z,t) = \int_0^t I(x,y,z)\eta(\tau)d\tau \tag{6}$$

The explicit function of $\eta(\tau)$ was calibrated through empirical data gathering during in-situ observations of voxel growth at different oxygen concentrations. As the exact value of the amount of diffused oxygen is not known, the calibration was done using data driven techniques by fitting the curve to the evolving cured profile over time, thus aligning with our formulated equation. Oxygen is quenched when energy is provided and is replenished over time. The replenishment time and quenching rate are related to the material properties of the resin. Using equation of the curve given in Fig. 7(a) and the growth rate equation for voxels, the efficiency of photopolymerization can be given by

$$\eta(\tau) = 1 - e^{-b\tau}$$

Where τ is the time and b is a material specific constant. For the resin in consideration, the value of b was experimentally computed to be 0.44.

Fig. 1(b) and (c) show two spatially close features generated as a result of sequential masks. If the time delay between the subsequent masks is small, the second feature tends to grow larger as shown in Fig. 1 (b). Conversely, if the time difference is large enough for oxygen levels to stabilize after diffusion, the second feature has the same size as the first feature. Fig. 1(c) shows two temporally sparse features bearing the same size despite being spatially close. The blue paraboloid shows the feature generated as a result of the first mask whereas the magenta paraboloid represents the feature generated as a result of the subsequent mask.

A 3D simulation was developed based on the aforementioned theories to study the pixel-pixel interactions in planar environment. The simulation model considered how pixels were arranged spatially, where they stood in relation to one another, and how their interactions affected certain attributes or phenomena of interest. The effects of pixel-pixel relationships on many characteristics such as voxel size, diffusion, or diffusion rates could be measured by simulating these interactions in a 3-D environment. Image processing algorithms like edge detection were used to trace the profile of the observed voxel and the datapoints were extracted from the detected edge. These were compared against the simulation results. Comparison with the observation data revealed that the developed simulations accurately model the voxel growth process with accuracy exceeding 95% and provide a robust tool for studying the light-resin interactions and process optimization.

The intricate nature of pixel-pixel interactions in planar structures was carefully examined using this 3D simulation. It provided a way to comprehend the underlying dynamics and mechanisms controlling how pixels behave in a three-dimensional, volumetric environment, offering crucial insights in the photopolymerization kinetics. Individual pixels are represented by green curve whereas the red curve represents the accumulated energy. Fig. 1(d) shows the spatial proximity effect in 3-D space and Fig. 1(e) shows the temporal proximity effect. When the features are temporally close, the voxels generated as a result of the second mask tend to grow larger. Magenta curve in Fig. 1(e) represents these larger features due to temporal proximity effect.

3. Experimental setup

The experimental setup consisted of two main components, a projection-based photocuring setup and an observation system consisting of a confocal microscope-based observation system for spatial observations from the top and a schlieren-based observation system for side-ways observation.

3.1. Digital light projection setup

This research uses an OmniCure S1500 UV mercury lamp system combined with a 405 nm UV filter for illumination. The light is delivered via a 0.37 NA light guide with a 3 mm output diameter, and all the experiments were performed at 40% light output, giving an irradiance of 462 μW/cm^2 and an exposure time of 6500 ms per exposure. Light coming from the lamp is collimated using a $f = 200$ mm achromatic doublet lens and was shone on a high-performance light engine from Vialux software used for digital mask generation. The DMD has a resolution of 1920×1080 with an individual micromirror measuring 10.8 μm on each side and a pitch of 1 μm. The light reflecting from the DMD was passed through a set of focusing lenses to form a focused image on the vat surface. The setup was compacted by using a flat mirror to deviate the light's path while providing the same optical distance. This setup allows tunability by changing the optics. Adjustable optics enable adaptable magnification for tuning the projected image. The optical system was adjusted to achieve a 1:5 magnification by using a 5x objective lens and later to achieve 1.5:1 magnification to test the system's robustness and study the proximity effect at varying scales. A bi-telecentric system was used for projection in both cases. A bi-telecentric system ensures constant magnification regardless of the distance or location in the field of view. Focused image is a critical aspect of these experiments as it aims at studying the light interactions amongst individual pixels. Along with the bi-telecentric system, high magnification camera as shown in Fig. 3 was used to ensure the projection focus. The designed system has very high resolution with the ability to resolve individual pixels. As the objective was to study the proximity effect in the spatial and temporal domain, a stationary platform submerged in the vat was used. Binary masks were projected from the bottom of the vat made from an all-side transparent UV-transparent cuvette. A high-speed CMOS camera from AmScope was used to capture the voxel growth process from the side, whereas a CCD camera from EIA Japan captured the spatial images from the top. A white LED with a light guide illuminated the schlieren setup.

Light reflecting off from each micromirror of the DMD in its 'on' state follows a 2D Gaussian energy distribution given by [29].

$$I_{i,j}(x,y) = P_{i,j}e^{-\left[\left(\frac{x}{a}\right)^2+\left(\frac{y}{b}\right)^2\right]} \tag{7}$$

Where P_{ij} is the peak power of the Gaussian function and a, b are the Gaussian radii, which for a single micromirror are considered equal. To find the light energy distribution for a multi-pixel mask image, Eq. (7) can be integrated across the exposed mask area. The Gaussian radius for a single pixel for the DMD used in our experiments is 4.97 μm. A single illuminated micromirror at 20% light output with an irradiance is 208 μW/cm^2 as seen from the camera is given in Fig. 2(a) and the corresponding intensity profile is given in Fig. 2(b). The full width half maximum (FMHW) for the Gaussian distribution is calculated to be 92% of the pixel size with a spreading (standard deviation) of approximately 39% of the pixel width.

3.2. Observation system

The observation setup consisted of two components, a schlieren-based system to observe the voxel growth from the side and a confocal system for spatial observations from the top. Schlieren exploits the changes in optical density of the resin as the polymerization progresses to give a detailed image of the voxel that is not easily visible to the naked eyes. A lens-based schlieren was used with a magnification system to observe the voxels from the side. The second component of the observation system consists of a confocal setup with a high magnification objective lens and a UV camera. The typical system has a UV camera and an objective lens placed at the focus of a $f = 15$ mm achromatic doublet lens on either side. As the photopolymerization progresses, there is a

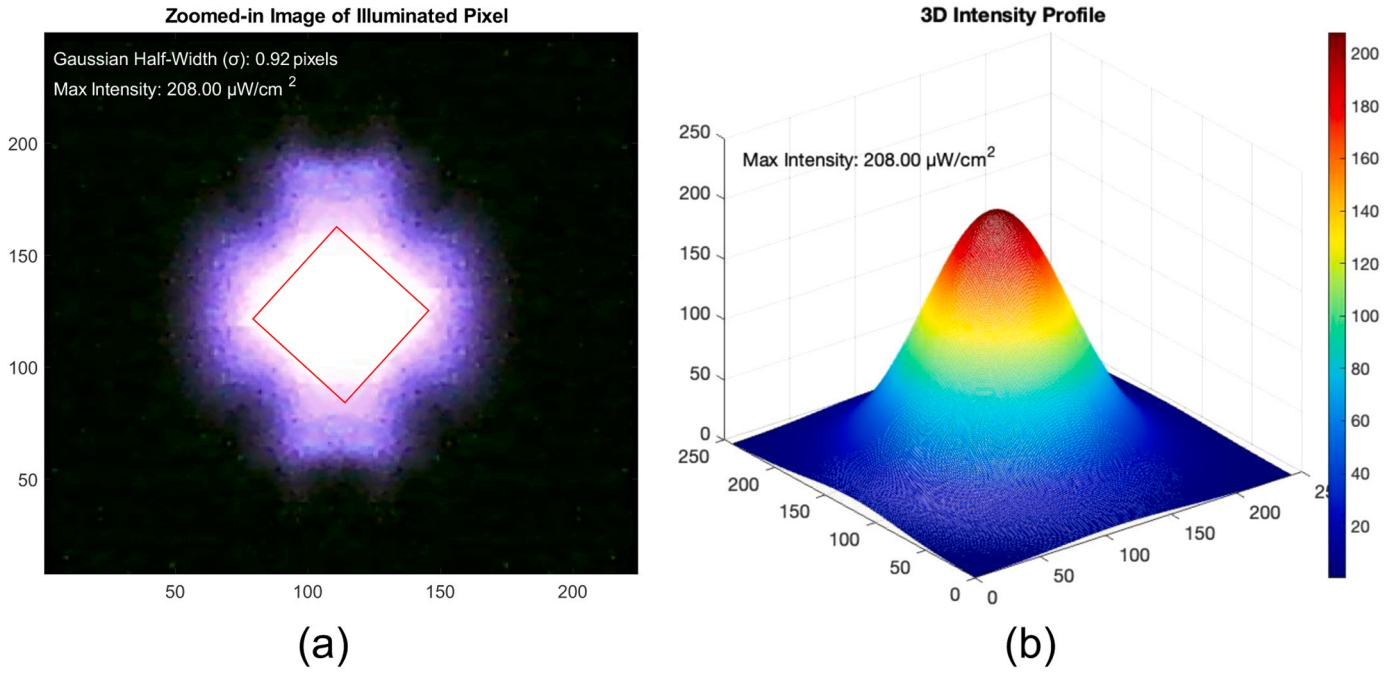

Fig. 2. (a) Zoomed-in image of the illuminated as seen from the high magnification camera. Red square represents the actual pixel size, and (b) 3D Gaussian intensity profile for the illuminated pixel.

local change in the optical density. This change causes the projected light to spread in the X-Y plane beyond the mask dimensions. A high-speed camera can capture this process frame by frame, and depending on the spread; the proximity effects can be quantified. We use a 405 nm UV filter, and the resin used for these experiments absorbs most of the UV light. A regular camera cannot detect the light transmitted through

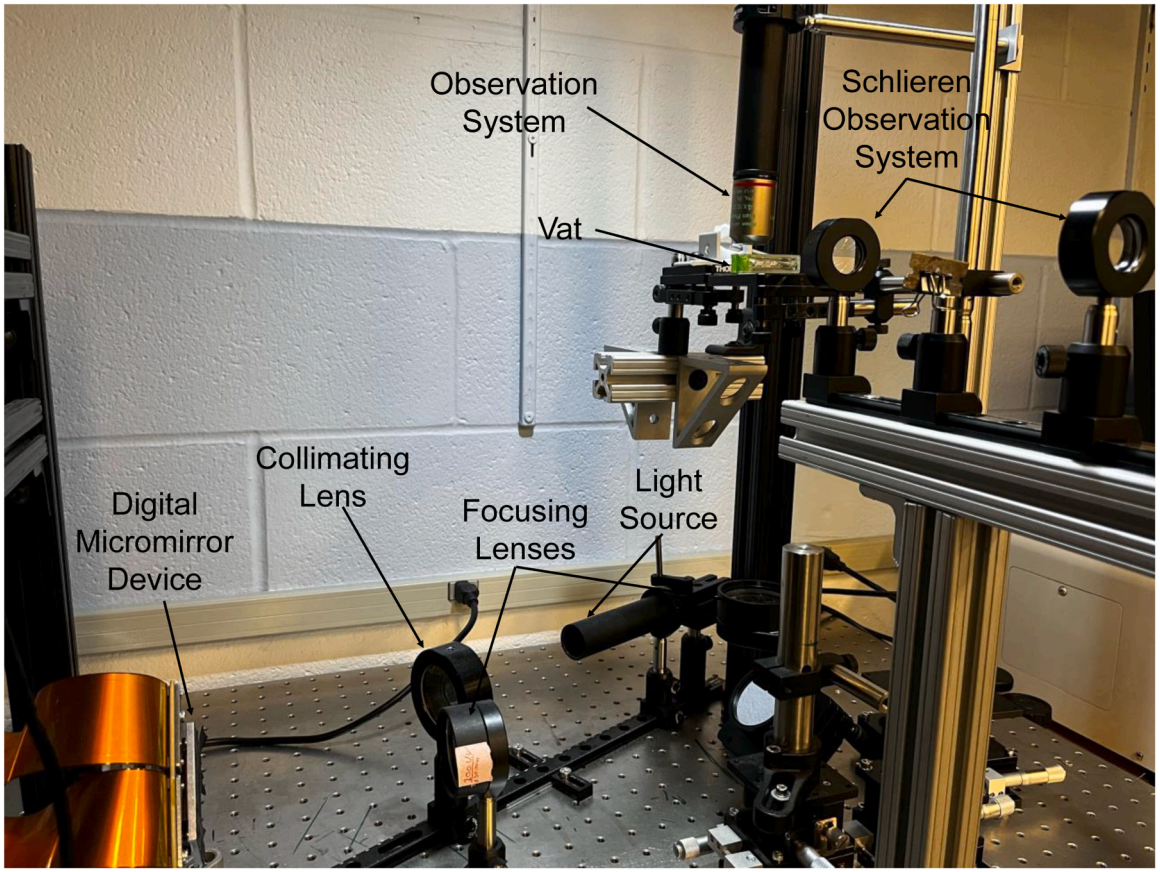

Fig. 3. UV based vat photopolymerization setup and the schlieren based observation system.

the resin, so a UV camera was used. A physical setup and schematic representation of the vat photopolymerization and the observation system are shown in Fig. 3 and Fig. S3 respectively. As shown, two sets of microscopic observation systems are deployed to capture the voxel growth process in lateral as well as spatial direction. The top observation system captures the photopolymerization process spatially by detecting the change in the focus based on the refractive index change.

The schlieren technique was developed in the early 1800 s which exploits the bending of light due to refractive index change corresponding to alterations in the optical density gradients in transparent media to generate images with contrast [30]. It is widely used to characterize fluid flows. A lens-based schlieren system as developed for this research has three main components: illumination source, lenses and knife-edge. The system uses collimated white light for illuminating the test area which is placed between the collimating lens and a pair of focusing lens. A knife-edge is placed at the focal point of the focusing lenses such that it cuts half the light passing through. When there is a change in the refractive index of the fluid in the test area corresponding to the resin polymerization, collimated light passing through it bends following Snell's law. When there is a change in the refractive index gradient, there is a corresponding shift in the light spot at the focus. This allows a local change in the number of rays that are blocked by the knife edge giving rise to a region of contrast depending on the bending direction and an image is generated on a virtual screen [31–33]. A camera with a confocal magnification setup is attached to the system as the parts under consideration are sub-50 μm.

4. Materials and methods

The acrylate-based resin was commercially procured from AnyCubic, and 2,4-Di-tert-butyl-6-(5-chloro-2 H-benzo-triazol-2-yl)phenol (Tinuvin 327) (procured from Sigma Aldrich) was used as a UV dye. 1% w/w dye was mixed with the resin by dissolving it in chloroform and stirring it at 500 rpm for 15 min. The printed samples were cleaned using 90% IPA followed by a bath of DI water inside a sonicator. To study the proximity effect in the spatial domain, binary masks with periodic patterns having different pitches were projected at a constant light intensity of 462 μW/cm^2. Temporal effects were studied by projecting two separate non-overlapping digital masks with a varying time delay between subsequent projections. The effect of oxygen was studied by preparing two additional samples. The oxygen-rich sample was prepared by bubbling supplemental oxygen into the resin for 60 s in a vacuum container to make sure supplemental oxygen was diffused into the resin. Another sample was deprived of oxygen by vacuuming out all the air and purging in carbon dioxide to displace oxygen. Additional carbon dioxide was poured into the vat and was sealed to avoid interactions with the atmospheric air.

The prepared photopolymer resin was exposed to five different energies using 405 nm UV doses to fabricate thin coupons. The curing depth was measured using a microscope measurement as discussed in our previous work [34]. The obtained C_d values were plotted against the logarithm of the input energy and a linear regression curve was fitted through the data (Fig. S4). Jacob's working curve holds that the penetration depth (D_p) is the slope of the curve whereas E_c is the x-intercept. E_c and D_p values corresponding to the light intensity of 462 μW/cm^2 were used for simulations.

5. Results and discussions

This section presents the experimental validation using the free-form voxel growth experiment. Particularly, the spatial spreading, cross-talking, temporal effects, and role of oxygen are measured and characterized using SEM.

5.1. Spatial effect

Feature density is the desired characteristic in the microfabrication of periodically patterned structures like microlens arrays or microneedles. Higher packing density has its advantages due to its unique optical and structural properties. Efforts are being made to fabricate high-resolution features as close as possible, but this comes at a cost. The spatial closeness of the features gives rise to cross-talking between the features. This effect is more prevalent in the proximity of the actual illuminated spot. It can be attributed to the light spreading into neighboring pixels, creating a halo around the actual projection, also known as the sphere of influence. The effect of cross-talk starts fading out when the spatial distance between the features increases.

Observations from the confocal microscopic system reveal this spatial effect in-situ. The experiments were repeated five times by changing the light intensity and exposure time. The total energy exposure was kept constant. While higher light intensity results in higher D_p, the overall profile of the cured parts was observed to be similar. These replicated experiments ensured that the results were consistent. It is seen that the neighboring features influence the part growth, and for the same exposure, the features that are in close proximity tend to grow bigger. Fig. 4(a) and (c) show the projected image, and Fig. 4(b) and (d) shows the observed image after 8 s of exposure. The halo around the features in Fig. 4(b) and (d) can be attributed to the scattering of light as the refractive index changes upon polymerization.

The cross-talking effect is more prevalent within a specific region and fades out as the spatial distance between the features increases. The light intensity distribution described by Eq. (1) follows an exponential pattern, indicating that as we move farther from the central point of the projected image, the light energy decays exponentially. As shown in Fig. 5(a), the spatial proximity effect decays exponentially and is not significant beyond 80 μm gap as the size deviation is well within the acceptable limits for the desired microlens applications. The decay function for spatial proximity was obtained by fitting the data using an exponential function represented by the general formula $N(d) = N_0 e^{-\lambda d}$ where $N(d)$ represents the size of the voxel with d units of spacing, N_0 is the size of the voxel when the spatial separation is the least, and λ is the decay constant which is determined iteratively. This is specific to this resin, but the overall trend is also similar for other materials. Fig. 5(b) shows sporadic connections between the features that arise due to the cross-talking between the neighboring features, and the effect seems to lessen as the gap between them increases. Fig. 5(d) is the control that has features as desired. Whereas Fig. 5(e) depicts the features that are smaller than desired for the same amount of exposure as they are sparsely spread, thus preventing any significant cross-talking from influencing the size.

The spatial cross-talking effect is evident only within a specific sphere of influence. It depends on the light intensity, light spreading, and the number of features present on either side. Fig. 6(a) shows a schematic of the additive effect of light bleeding into neighboring pixels. The features in the center are influenced by the light from its eight immediate neighbors. The features on the sides are influenced by five neighbors, whereas the features on the corners get contributions only from three of its neighbors. This non-uniformity in the exposure is more prevalent within the sphere of influence and is dependent on the chemical composition of the resin, wavelength of light, and the depth of focus [13]. When the gap between the individual features is more than a certain value, the additive effect of light intensity is not very predominant. The distance beyond which the additive effect weakens is generally determined by the chemical properties of the resin. Based on the UV resin used in these experiments, the effect is more prevalent when the gap between adjacent features is relatively small. Fig. 6(b) shows the non-uniformity in the size of the printed microlens at the corner. This can be attributed to the fact that for all the other lenses, the size is due to the additive effect of light from all the neighbors. Whereas for the

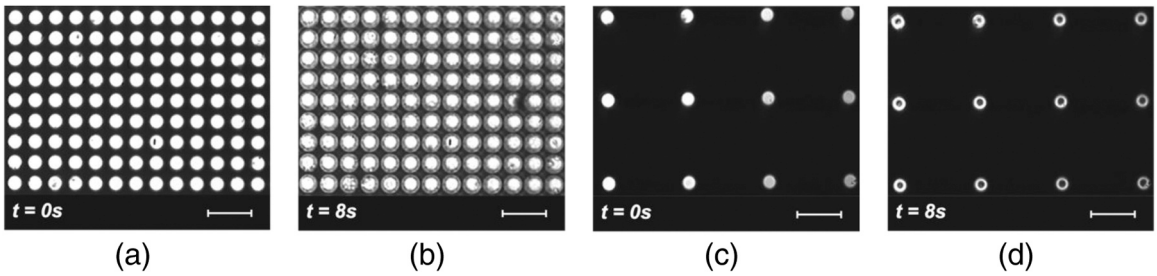

Fig. 4. Spatial proximity effect as observed from the designed system for a feature size of 20 μm (a) pitch = 20 μm, (b) polymerized part, (c) pitch = 200 μm, and (d) polymerized part. Scale bar = 50 μm.

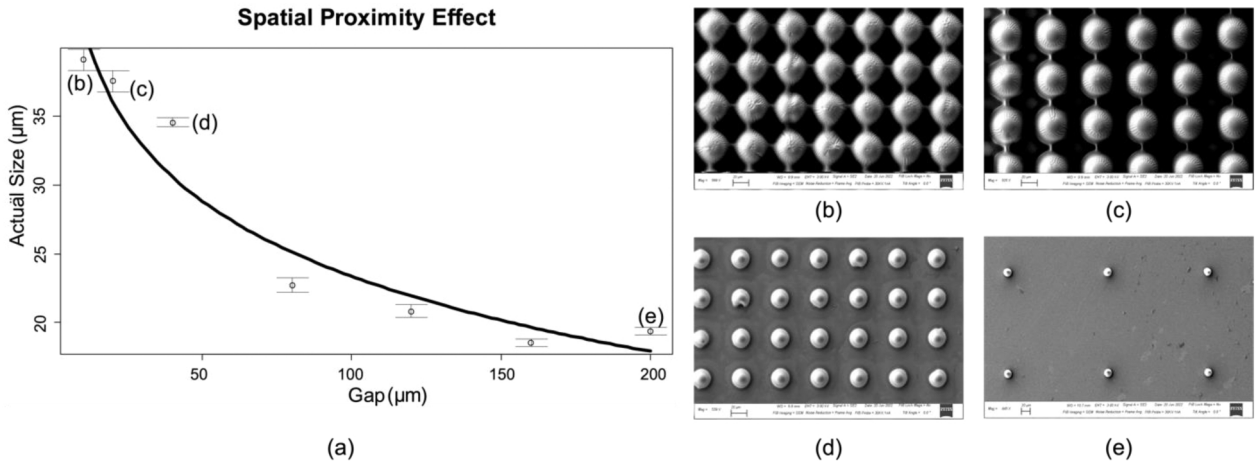

Fig. 5. (a) Graph showing how spatial effect decays as the inter-feature gap increases with error bars for size measurement, features with different pitch as observed under SEM (b) pitch = 10 μm (c) pitch = 20 μm (d) pitch = 40 μm (e) pitch = 200 μm (SEM scale bar = 20 μm).

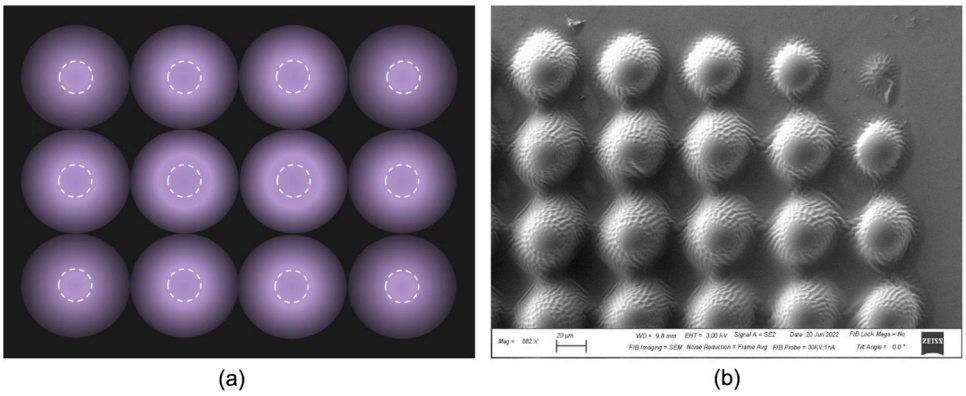

Fig. 6. (a) Schematic of light bleeding into neighboring pixels in the spatial domain where the dashed white line represents the projected image (b) SEM image depicting spatial proximity effect at corners (SEM scale bar = 20 μm).

microlens at the corner, the neighboring features exist only on one side.

5.2. Temporal effect

As discussed in the previous section, the spatial proximity effect has made the adoption of vat photopolymerization in microfabrication challenging and efforts need to be made to find alternatives to overcome this effect. Using sequential masks with alternating patterns is a possible way to circumvent the spatial proximity effect. In this method, multiple masks with larger spatial gaps and alternating feature locations are projected sequentially. Both the projected masks have similar exposure times and light intensity combinations to ensure that the same amount of energy is provided in both exposures. The experiments were repeated three times to eliminate the effect of ambient conditions and ensure consistency. Fig. 7(b) and (c) show the masks for the first and second projections. The masks have patterns at alternating locations. The dotted lines in Fig. 7(c) are representative of the cured features and are not a part of the actual mask. Ideally, we should take advantage of breaking the sphere of influence and prevent the effect of light bleeding. Despite this being a great alternative, in practice, the time delay between two projections plays a critical role in determining the feature resolution. Experiments have shown that if the delay between subsequent projections is small, the second projection tends to absorb more energy resulting in thicker features. This is termed the proximity effect in the

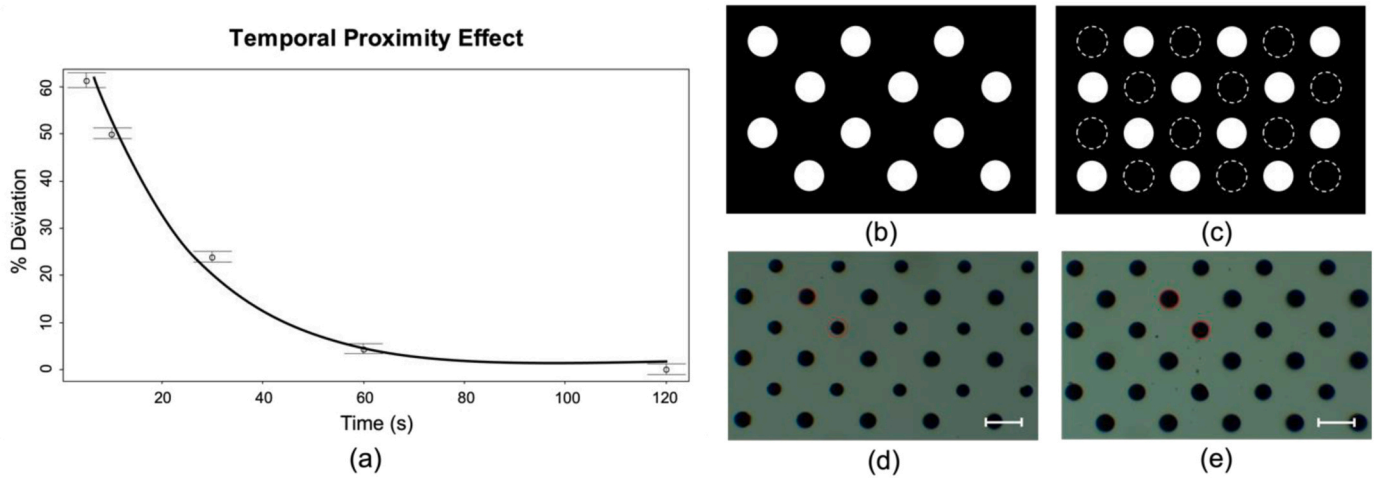

Fig. 7. (a) Graph showing how the temporal effect fades out with time, (b) mask for first exposure, (c) mask for second exposure, temporal effect as seen under microscope when (d) time delay is 10 s, and (e) time delay is 60 s (red circle represents the actual part) (Scale bar = 50 μm).

temporal domain or simply the temporal effect.

The temporal proximity effect fades out as the time delay increases and behaves like a closely packed single projection. Fig. 7(a) shows the exponential decay of the temporal effect as the time delay between projections increases. The graph represents the percentage deviation in size between the features printed from the first and second projections. As seen from Fig. 7(b), when the time difference is small, the features printed due to the second projection tend to be relatively larger. It can be seen from Fig. 7(c) and (e) that with increased delay, the features are visually indistinguishable, and there is an increase in the uniformity of the features. It is also evident that planning the images with alternating patterns helps overcome undesired effects like feature broadening seen in single projection images.

5.3. Effect of oxygen inhibition

Oxygen inhibition has long plagued free-radical polymerization processes. Molecular oxygen scavenges the free radicles and either prolongs the photocuring process or altogether inhibits it depending on the amount of dissolved oxygen and the provided energy. It is known to react with active radicals and generate dead chain ends, thus preventing reaction propagation [35,36]. This issue is more pronounced in low intensity curing processes that use UV cure, such as the one used in this research. As discussed in the previous section, oxygen inhibition is one of the main causes for the temporal effect. During the first exposure, a part of the energy is used to scavenge the oxygen free radicals present in the resin. If the time delay is small enough to replenish the consumed oxygen, all of the input energy is used for photopolymerization resulting in thicker features. This is dependent on resin viscosity, available oxygen, irradiation, and thermal effects. Fig. 7(a) shows the decay function of oxygen inhibitory effects. It is necessary to either account for the dissolved oxygen while modeling the process or find ways to eliminate the oxygen. Despite the relative maturity of vat photopolymerization printing, this effect has not yet been quantified.

There are numerous physical and chemical ways to reduce oxygen inhibition. Using higher viscosity polymers or increasing the exposure time by slower cure speeds can help mitigate this effect [37,38]. Prolonged curing at lower irradiance is not always viable as it can lead to longer printing times, which is not desirable. Other potential ways of mitigating oxygen inhibition are increasing the free radical concentration by increasing the photoinitiator concentration or by increasing the UV intensity. While increasing the photoinitiator concentration is possible, it is not always practical, especially in commercial resins. UV intensity augmentation magnifies the sphere of influence by light bleeding, thus giving rise to spatial proximity effects. Removing oxygen from the cure zone by displacing it with inert gas can help mitigate the effect without chemically transforming the resin or increasing energy requirements. Fig. 8(b) shows that when the amount of dissolved oxygen is higher, the printed features are about 15% smaller than the control in Fig. 8(a). This can be attributed to the fact that more energy is consumed to quench the oxygen requiring a longer exposure to overcome the energy barrier, resulting in weaker propagation chains that take longer to polymerize. On the other hand, the features in the oxygen-deprived environment, as seen in Fig. 8(c), are approximately 32% larger as more energy is available for actual polymerization.

As discussed in the previous section, the temporal effect stems from the oxygen inhibitory properties. When the time delay is more, it allows for more time to replenish the oxygen used during the first exposure, thus returning the resin to the status quo, and giving rise to uniform features. On the other hand, when the time delay is short, the oxygen consumed during the first exposure is not restored, thus utilizing most of the energy from the second exposure for polymerization, giving rise to thicker features, as seen in Fig. 9(b). When the resin is deprived of oxygen, the effect is much more subtle, even when the time delay is small. Fig. 9(c) shows the results after repeating the sequential exposure experiment with a 10 s delay in an oxygen-deprived resin. The minute non-uniformity in the parts from the two exposures might be because of the process limitations to eliminate all of the oxygen. Though the spatial effect discussed in the previous sections primarily arises due to the light bleeding into neighboring pixels, we believe oxygen too plays a role. When the features are closely packed, the effective energy per unit area is more, causing the oxygen to get quenched faster, thus leaving more energy available for actual polymerization. On the other hand, when the gap between the features is more prominent, it takes longer for the oxygen to get consumed as the energy density is lower, thus giving smaller than desired features for the same exposure. This can also explain why polymerization is difficult when the feature size gets smaller.

5.4. Validation and robustness

The proximity effect is more pronounced at micron scale, but it exists at larger scale as well. Experiments were conducted to observe this effect at macro scale to validate our claims and demonstrate the robustness of our designed system. Vat photopolymerization setup used in this research allowed us to change the magnification of the system to 1.5:1. PEGDA 250 UV resin was used for this experiment. The designed schlieren setup allowed us to observe the polymerization process from the side and revealed how the proximity effect takes place. Voxel growth dynamics were studied for macro scaled parts using the designed schlieren system.

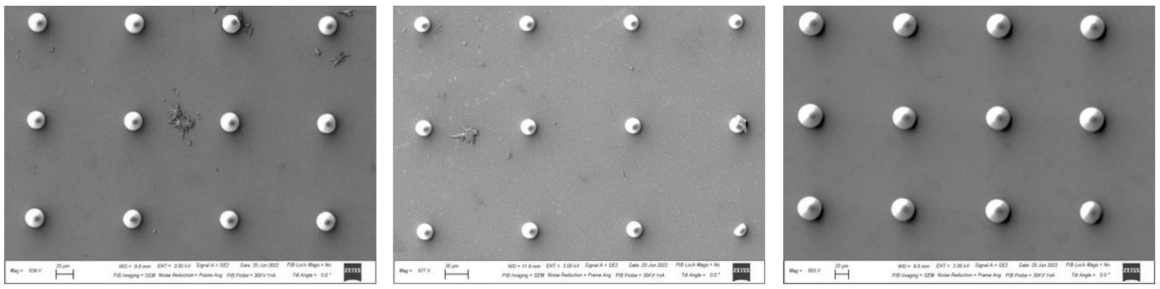

Fig. 8. Effect of oxygen as seen in the spatial domain for (a) stock/control resin, (b) resin with an oxygen-rich environment, and (c) resin with an oxygen-deprived environment. (SEM scale bar = 20 μm for (a) and (c), and 30 μm for (b)).

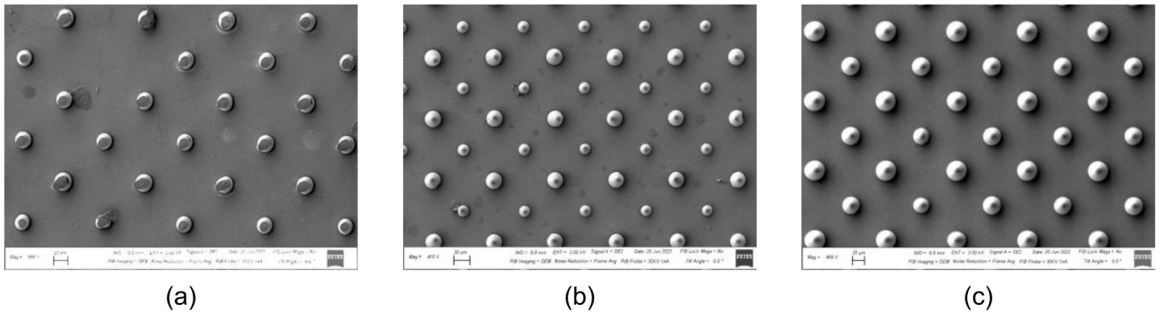

Fig. 9. Temporal effect of proximity (a) with control/stock resin time delay 60 s, (b) with control/stock resin time delay 10 s, and (c) with oxygen-deprived resin time delay 10 s (SEM scale bar = 20 μm).

Fig. 10 shows the voxel growth at different time stamps during vat polymerization for a 100 μm feature. Fig. 10 (a), (b), and (c) represent the voxel growth during the first projection. They show the nonlinear photopolymerization process that is terminated at 5 s. To study the temporal effect, a second mask was projected with alternating patterns after a time delay of 10 s Fig. 10 (d), (e), and (f) represent the voxel growth during second exposure. As evident from the images the growth rate during second exposure is much faster as most of the energy is utilized for polymerization rather than oxygen quenching. For the same exposure, the voxels from the second projection are relatively larger. The schlieren system allowed us to characterize this process in-situ thus eliminating the discrepancies that might occur during cleaning post processing.

The simulations in Fig. 11 agree well with the experimental findings. Fig. 11 (a-c) depict the voxel growth caused by the first mask, where the magenta curves represent individual pixels, and the red curve represents the accumulated energy resulting from all illuminated pixels. The actual voxel is depicted in blue. On the other hand, Fig. 11 (d-f) showcase the voxel growth caused by the second mask, which was projected with a time delay as implemented in the experiments. The cyan curves represent the pixels of the second mask, while the voxel is depicted by the magenta curve. Despite the same irradiance, the voxels grow larger due to the short time delay, which encompasses the temporal proximity effect.

6. Applications

Microlenses are garnering increased attention in opto-electronics, biomedical, and sensing applications. Fabrication of these microlenses need to meet stringent requirements for surface quality, uniformity, and

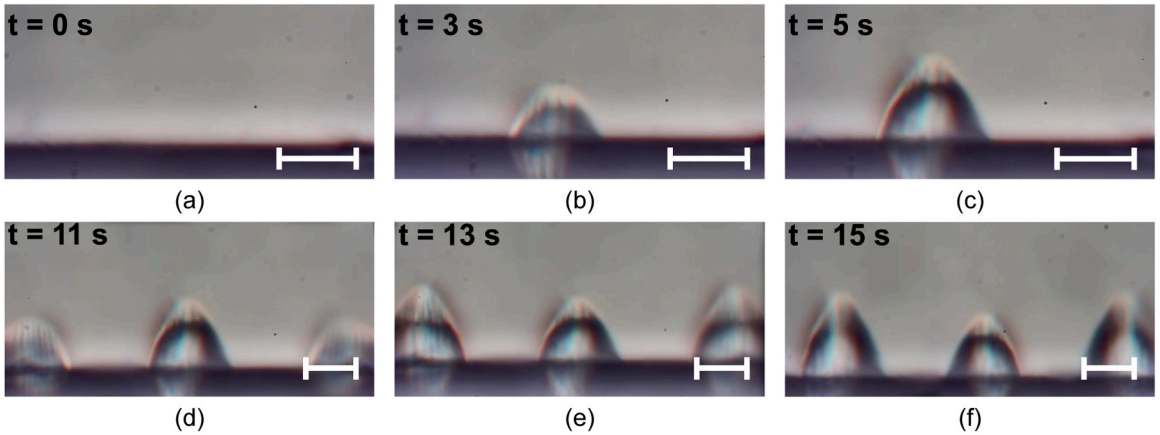

Fig. 10. Temporal proximity effect observed from the side at different time stamps. (a), (b), and (c) represent the voxel growth resulting from the first mask whereas (d), (e), and (f) represent the voxel growth resulting from the second mask projected after a 5 s delay. (Scale bar = 100 μm).

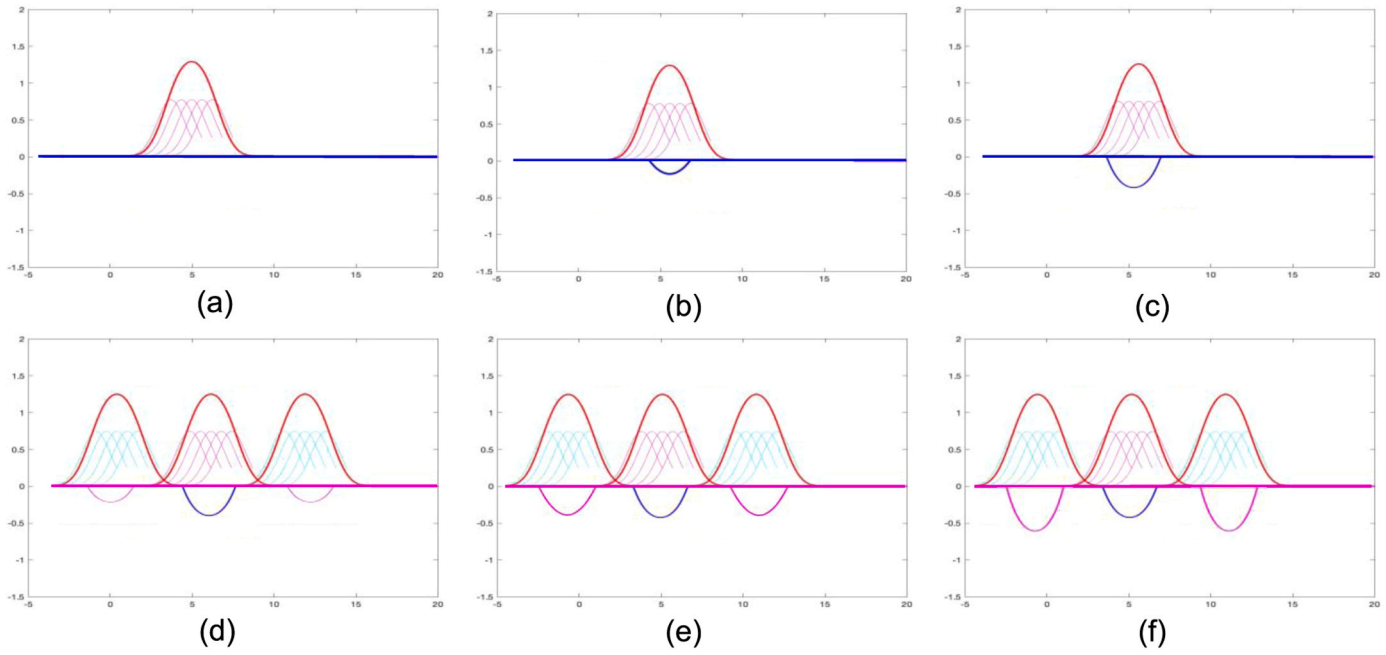

Fig. 11. Simulations for temporal effect. Blue paraboloid represents the cured part from the first mask and magenta paraboloid represents the cured part from the second mask.

precision. Various manufacturing techniques like hot embossing, laser engraving, thermal reflow, micromachining, vat photopolymerization, etc. have been developed over the past few decades to address these requirements [39]. However, despite the relative maturity of these techniques, certain limitations like low throughput, long processing times, and challenges associated with the quality control still persist.

Efforts are underway to overcome these limitations and further advance the manufacturing of microlenses. Advancements in additive manufacturing hold promise in achieving faster and more precise microlens fabrication. Vat photopolymerization technique is gaining popularity due to its high throughput, high resolution, low costs, and superior consistency. It constructs freeform 3D shapes with selective polymerization of UV resin in a layer-by-layer format. As the illuminated mask is generated by controlling millions of high frequency micro-mirrors, pixel scale modulation is possible. This makes it ideal process for high resolution manufacturing. Layer by layer technique generates staircase pattern which isn't ideal for micro-optical components [40]. Use of single exposure strategies is becoming increasingly popular, especially for fabricating sub 100 μm microlenses. Being a layer-less technique, it is void of any moving parts thus providing high fidelity and throughput. Single exposure strategies have been implemented by many researchers in conjunction with either dynamic focal adjustment or oscillation assisted surface smoothening [1,41]. While these techniques are capable of achieving the desired optical as well as surficial requirements, they are not suitable for on-the-fly modifications and cannot guarantee consistency when the microlens placement is randomized. Random microlens placement is desired to eliminate grating diffraction. Observation based empirical models were introduced in our previous work to better predict the profile of the generated microlens [28].

An image was generated with densely packed binary circular patterns for generating a microlens array. As seen in Fig. 12 (a) the microlenses are arranged in a high-density randomized pattern. As the gap between the individual microlenses is non-uniform, determining the appropriate exposure time is challenging. A longer exposure can lead to unnecessary interconnects being formed between the closely spaced lenses whereas a shorter exposure may mean that some lenses are not fully cured. The 3D simulation developed based on the observed results and the discussed theory showcases the connections between the closely spaced patterns. It can be seen that for the same irradiance, circles with smaller gap generated undesirable interconnects whereas features that were sparse were underdeveloped. This can be attributed to the

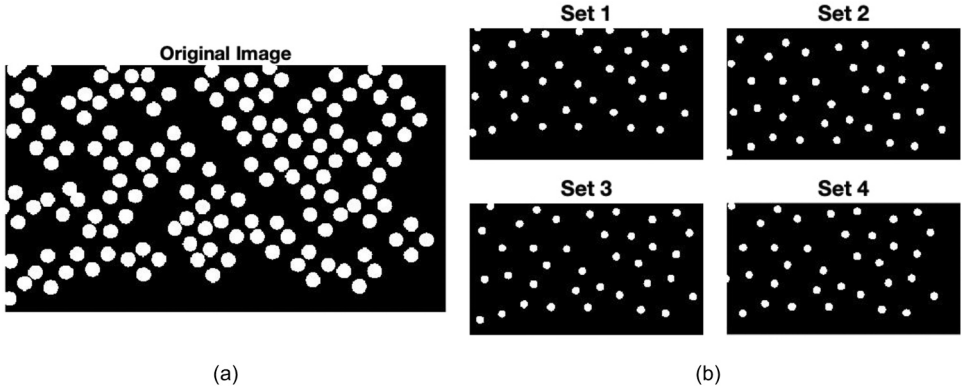

Fig. 12. (a) Mask image for densely packed microlens array, (b) set of independent images that can be projected sequentially to achieve the same mask as the original one after overlapping.

proximity effect.

A multi-mask strategy was developed to overcome the challenges associated with proximity effects in vat photopolymerization based printing. We have deployed an algorithm that segments the image with dense features into separate images based on the inter-feature distance. This approach combines empirical models and the understanding of proximity effect to address the issues effectively. It starts by identifying the features and calculates the distance between the centroids. A sphere of influence is calculated around each feature based on the irradiance parameters and a densely packed image is generated by merging multiple images with sparsely spaced features. It then divides the image into multiple such images by considering the sphere of influence for spatial and temporal cross-talking. The spatial proximity effect is eliminated by maintaining adequate inter-feature spacing in each mask image. In addition to the spatial considerations, an image planning strategy was developed to tackle issues caused by temporal proximity. This involves determining the appropriate exposure time and delay between subsequent projections. By calculating the optimal delay between the projections based on the decay function as shown in Fig. 7(a), the potential for interference between features due to temporal proximity can be minimized. The number of such images generated is optimized to minimize the overall curing time and the temporal spacing between subsequent projections. The resulting image planning strategy ensures precise and well-defined features in the final printed image.

Print resolution can be significantly improved by implementing the optimized multi-mask strategy. An enhanced accuracy and resolution can be achieved by effectively merging both spatial and temporal proximity effects, resulting in a higher-quality printed array. Use of a single mask with densely packed features as shown in Fig. 12 (a) results in uneven curing. Features that are in spatial proximity tend to grow abnormally larger and tend to form shapes that gravitate towards neighboring features. This leads to undesirable interconnects as seen in Fig. 13 (a). An optimized multi-mask strategy with appropriate exposure planning can overcome this issue. Fig. 12 (b) illustrates the original mask image divided into four independent images that are sequentially projected. The printed microlens array as shown in Fig. 13 (b) demonstrates the effectiveness of the proposed multi-mask strategy in achieving improved print resolution and overall print quality.

7. Discussion and future work

A substantial portion of prior research on investigating the proximity effect has been primarily constrained to scanning or laser-based systems. Studies on pixel blending such as those conducted by Zhou et.al. have predominantly revolved around macro-scaled voxels. However, it is crucial to recognize that the voxel growth dynamics at the micron scale differ significantly due to variation in the available energy and the threshold for overcoming oxygen inhibition. Models tailored for macro-scaled systems might not consistently hold true when applied at micron scale. Our approach is novel as it has pioneered a schlieren based observation system, enabling real-time observation of the voxel growth process, and furnishing observational evidence of the proximity effect and elucidates the intricacies of the proximity effect. Temporal proximity effect has been observed for the first time. This observational data has been used to develop simulation models for predicting the voxel growth process and ultimately aid in image planning strategies.

In this paper, we investigated the proximity effects in spatial and temporal scales during vat photopolymerization using experimental data at micron scale. Different patterned structures were exploited to study the influence of structural features in vat photopolymerization on a temporal and spatial scale. The measurements indicate that light spreading in the sphere of influence strongly affects the material response. The spatial response extends beyond the actual projections when the feature density is high, as each feature is influenced by its immediate neighbors. The temporal effect arises when multiple projections are used subsequently and were seen to have an effect within a specific period. We also studied the role of oxygen in free radical polymerization. It was observed that the amount of oxygen was one of the influential factors in determining the feature dimensions, and oxygen inhibition is one of the causes for the temporal effect. The research also, for the first time, demonstrates techniques for observing the voxel growth and the interactions between adjacent features in-situ. The temporal proximity as observed from the schlieren system has opened up new possibilities for developing data driven models specific to patterned periodic structures that consider the inter-feature interactions.

The optimized multi-mask strategy, considering the photopolymerization kinetics and the observed proximity effect, offered enhanced control and tunability in the fabrication of microstructure arrays using a single-exposure layer-less photopolymerization technique. By understanding the photopolymerization process and its relationship with the proximity effect, the exposure energy could be finely adjusted and optimized. This improved controllability allowed for the precise fabrication of microstructures, resulting in high-quality and well-defined arrays. Better tunability of the exposure energy improved the controllability of the fabricated microstructure array using single exposure layer-less photopolymerization technique. This optimized approach to multi-mask fabrication using the layer-less photopolymerization technique opens up new possibilities in the field of microstructure array fabrication. It offers improved controllability, enabling the production of intricate and customized structures for various applications in fields such as microelectronics, photonics, and biotechnology. The tools provided in this work have opened new avenues in understanding the voxel growth mechanisms and propelled us towards developing strategies for improving the resolution of vat photopolymerization process.

The simulations developed in this work build upon the Beer-

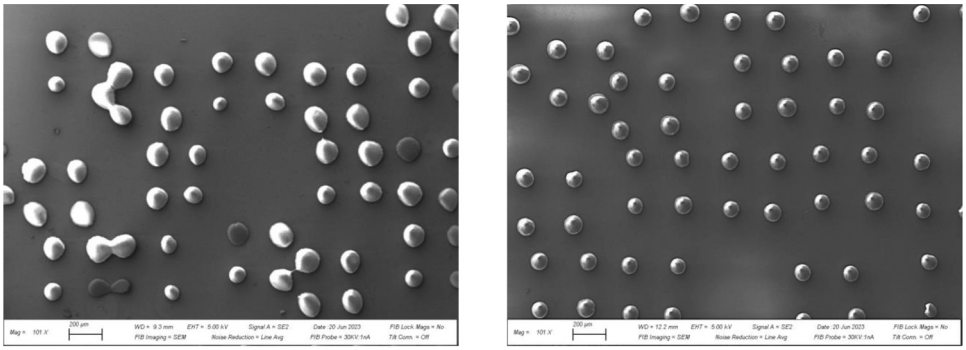

(a) (b)

Fig. 13. SEM images for (a) Printed microlens array using a single densely packed mask, (b) microlens array printed using an optimized multi-mask strategy (Scale bar = 200 μm).

Lambert's equations and data driven approaches from the observed voxel growth process to combine the effect of oxygen and other chemical properties. It is important to note that while our present study primarily aims to acknowledge the existence of spatial and temporal proximity effects, the simulation models we have developed are still at a nascent stage. We view this work as a steppingstone towards more comprehensive simulations. Although oxygen inhibition also affects the spatial proximity effects, further experiments need to be conducted to pinpoint the significant contributor, radical and/or oxygen, to this proximity effect. This research doesn't consider thermal effects that might play a role in determining the spatio-temporal proximity characteristics. While the research work successfully demonstrated fabrication of high-density microlens array, more data needs to be collected to derive an even robust empirical models from showcasing how the photopolymerization process takes place in single-shot vat photopolymerization printing. This research has paved the way toward developing optimization models for printing densely packed high-resolution micron scaled features with enhanced uniformity and tunability. Our forthcoming research is centered on the creation of robust simulation models that combine physics-based approaches with data-driven techniques. We anticipate that these advanced models will significantly contribute to process optimization and image planning, particularly in the context of high-resolution projection micro stereolithography for high-density feature fabrication. The work can be further extrapolated in multi-layer 3D printing applications in achieving controlled porosity, intricate infills, and optimized supports.

CRediT authorship contribution statement

Aditya Chivate: Writing – review & editing, Writing – original draft, Visualization, Validation, Software, Methodology, Investigation, Formal analysis, Data curation. **Zipeng Guo:** Writing – review & editing, Validation, Investigation. **Chi Zhou:** Writing – review & editing, Supervision, Software, Resources, Project administration, Methodology, Investigation, Funding acquisition, Conceptualization.

Declaration of Competing Interest

The authors declare that they have no known competing financial interests or personal relationships that could have appeared to influence the work reported in this paper.

Data availability

Data will be made available on request.

Acknowledgments

The authors would like to gratefully acknowledge the support from the National Science Foundation (NSF) through grant ECCS-2111056.

Appendix A. Supporting information

Supplementary data associated with this article can be found in the online version at doi:10.1016/j.addma.2023.103926.

References

[1] C. Yuan, et al., Ultrafast three-dimensional printing of optically smooth microlens arrays by oscillation-assisted digital light processing, ACS Appl. Mater. Interfaces 11 (43) (2019) 40662–40668.
[2] Y. Li, et al., Bioinspired functional surfaces enabled by multiscale stereolithography, Adv. Mater. Technol. 4 (5) (2019), 1800638..
[3] C. Yan, et al., 3D printing of bioinspired textured surfaces with superamphiphobicity, Nanoscale 12 (5) (2020) 2924–2938.
[4] S.R. Dabbagh, et al., 3D-printed microneedles in biomedical applications, Iscience 24 (1) (2021), 102012.
[5] A.S. Cordeiro, et al., Two-photon polymerisation 3D printing of microneedle array templates with versatile designs: application in the development of polymeric drug delivery systems, Pharm. Res. 37 (9) (2020) 1–15.
[6] J.K. Hohmann, et al., Three-dimensional μ-printing: an enabling technology, Adv. Opt. Mater. 3 (11) (2015) 1488–1507.
[7] H.-B. Sun, S. Kawata, Two-photon photopolymerization and 3D lithographic microfabrication, NMR 3D Analysis Photopolym. (2004) 169–273.
[8] G. Weisgrab, et al., 3D printing of large-scale and highly porous biodegradable tissue engineering scaffolds from poly (trimethylene-carbonate) using two-photon-polymerization. Biofabrication 12 (4) (2020) 045036..
[9] Z. Huang, et al., Two-photon polymerization nanolithography technology for fabrication of stimulus-responsive micro/nano-structures for biomedical applications, Nanotechnol. Rev. 9 (1) (2020) 1118–1136.
[10] J.-W. Choi, Y. Lu, R.B. Wicker, Projection microstereolithography as a micro-additive manufacturing technology, Addit. Manuf. Innov. Adv. Appl. 4 (2015) 101..
[11] C. Arnoux, et al., Understanding and overcoming proximity effects in multi-spot two-photon direct laser writing, Addit. Manuf. 49 (2022), 102491.
[12] D. Tan, et al., Reduction in feature size of two-photon polymerization using SCR500. Appl. Phys. Lett. 90 (7) (2007), 071106..
[13] E.H. Waller, G. Von Freymann, Spatio-temporal proximity characteristics in 3D μ-printing via multi-photon absorption. Polymers 8 (8) (2016) 297..
[14] Zhou, C., Chen Y., and Waltz R.A., 2009. Optimized mask image projection for solid freeform fabrication. in International Design Engineering Technical Conferences and Computers and Information in Engineering Conference.
[15] Zhou, C., et al., 2009. Optimized mask image projection for solid freeform fabrication. 131(6).
[16] C. Zhou, Y. Chen, Additive manufacturing based on optimized mask video projection for improved accuracy and resolution, J. Manuf. Process. 14 (2) (2012) 107–118.
[17] H.-W. Kang, J.H. Park, D.-W. Cho, A pixel based solidification model for projection based stereolithography technology, Sens. Actuators A Phys. 178 (2012) 223–229.
[18] C. Sun, et al., Projection micro-stereolithography using digital micro-mirror dynamic mask, Sens. Actuators A Phys. 121 (1) (2005) 113–120.
[19] M.M. Emami, M. Jamshidian, D. Rosen, Multiphysics modeling and experiments of grayscale photopolymerization with application to microlens fabrication, J. Manuf. Sci. Eng. 143 (9) (2021), 091005..
[20] Emami, M.M. and Rosen D.W., 2018. An improved vat photopolymerization cure model demonstrates photobleaching effects. in Solid Freeform Fabrication Symposium (Austin, TX).
[21] M.M. Emami, D.W. Rosen, Modeling of light field effect in deep vat polymerization for grayscale lithography application, Addit. Manuf. 36 (2020), 101595.
[22] S.M. Montgomery, et al., Pixel-level grayscale manipulation to improve accuracy in digital light processing 3D printing. Adv. Funct. Mater. (2023), 2213252..
[23] R. Setter, et al., Modeling of the curing kinetics of acrylate photopolymers for additive manufacturing, Polym. Eng. Sci. (2023).
[24] K. Taki, A simplified 2D numerical simulation of photopolymerization kinetics and oxygen diffusion–reaction for the continuous liquid interface production (CLIP) system, Polymers 12 (4) (2020) 875..
[25] C. Zhou, Y. Chen, Calibrating large-area mask projection stereolithography for its accuracy and resolution improvements. 2009 International Solid Freeform Fabrication Symposium, University of Texas at Austin, 2009.
[26] C. Zhou, H. Xu, Y. Chen, Spatiotemporal projection-based additive manufacturing: a data-driven image planning method for subpixel shifting in a split second, Adv. Intell. Syst. 3 (12) (2021), 2100079..
[27] P.F. Jacobs, Rapid Prototyping & Manufacturing: Fundamentals of Stereolithography, Society of Manufacturing Engineers, 1992.
[28] A. Chivate, C. Zhou, Enhanced schlieren system for in situ observation of dynamic light–resin interactions in projection-based stereolithography process, J. Manuf. Sci. Eng. 145 (8) (2023), 081005..
[29] Z. Xiong, et al., Illumination uniformity improvement in digital micromirror device based scanning photolithography system, Opt. Express 26 (14) (2018) 18597–18607.
[30] G.S. Settles, Schlieren and shadowgraph techniques: visualizing phenomena in transparent media, Springer Science & Business Media, 2001.
[31] C. Huang, J.W. Gregory, J.P. Sullivan, A modified schlieren technique for micro flow visualization, Meas. Sci. Technol. 18 (5) (2007) N32..
[32] S. Agarwal, et al., On refractive optical flow. European Conference on Computer Vision, Springer, 2004.
[33] Mazumdar, A., 2013. Principles and techniques of schlieren imaging systems.
[34] Z. Guo, et al., 3D-printed electrically conductive silicon carbide. Addit. Manuf. 59 (2022), 103109.
[35] J. Mandal, K. Zhang, N.D. Spencer, Oxygen inhibition of free-radical polymerization is the dominant mechanism behind the "mold effect" on hydrogels, Soft Matter 17 (26) (2021) 6394–6403.
[36] S.C. Ligon, et al., Strategies to reduce oxygen inhibition in photoinduced polymerization, Chem. Rev. 114 (1) (2014) 557–589.
[37] Schwalm, R., 2006. UV coatings: basics, recent developments and new applications.
[38] C.B. Jo Ann Arceneaux, Kevin Poelmans Use of Amino Acrylates to Reduce Photoinitiator Concentration Or Increase Cure Speed in UV LED-Curable OPVs and Flexo Inks, Paint & Coating Industry: PCI Mag, 2018.

[39] W. Yuan, et al., Fabrication of microlens array and its application: a review, Chin. J. Mech. Eng. 31 (1) (2018) 1–9.
[40] Y. Gao, et al., Research on dynamical-gradual greyscale digital mask lithography, J. Mod. Opt. 58 (7) (2011) 573–579.
[41] P.-C. Chen, C.-S. Yeh, C.-Y. Hsieh, Defocus digital light processing stereolithography for rapid manufacture of microlens arrays, Sens. Actuators A Phys. 345 (2022), 113819.